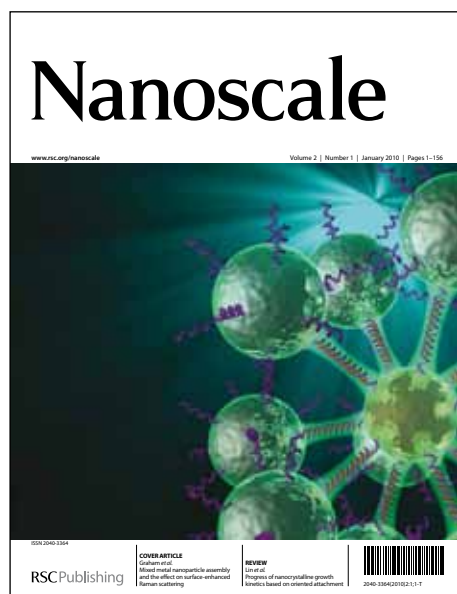


# Nanoscale

Accepted Manuscript



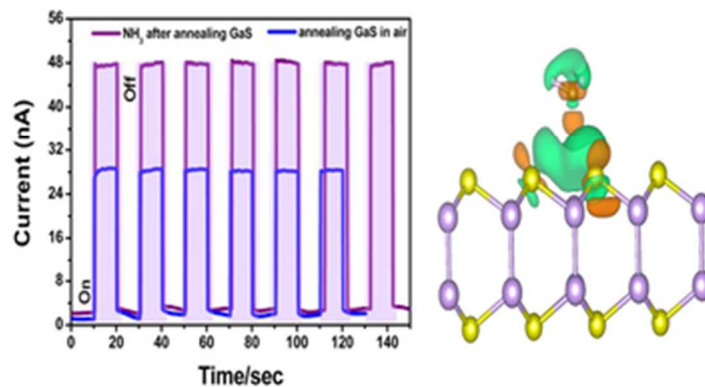
This is an *Accepted Manuscript*, which has been through the RSC Publishing peer review process and has been accepted for publication.

*Accepted Manuscripts* are published online shortly after acceptance, which is prior to technical editing, formatting and proof reading. This free service from RSC Publishing allows authors to make their results available to the community, in citable form, before publication of the edited article. This *Accepted Manuscript* will be replaced by the edited and formatted *Advance Article* as soon as this is available.

To cite this manuscript please use its permanent Digital Object Identifier (DOI®), which is identical for all formats of publication.

More information about *Accepted Manuscripts* can be found in the [Information for Authors](#).

Please note that technical editing may introduce minor changes to the text and/or graphics contained in the manuscript submitted by the author(s) which may alter content, and that the standard [Terms & Conditions](#) and the [ethical guidelines](#) that apply to the journal are still applicable. In no event shall the RSC be held responsible for any errors or omissions in these *Accepted Manuscript* manuscripts or any consequences arising from the use of any information contained in them.



Few-layer GaS two-terminal photodetector with fast and stable response has been prepared, and it exhibited different response in various of gas environment.  
29x16mm (300 x 300 DPI)

Cite this: DOI: 10.1039/c0xx00000x

www.rsc.org/xxxxxx

ARTICLE TYPE

# High performance few-layer GaS photodetector and its unique photo-response in different gas environment

Shengxue Yang<sup>a</sup>, Yan Li<sup>a</sup>, Xiaozhou Wang<sup>b</sup>, Nengjie Huo<sup>a</sup>, Jian-Bai Xia<sup>a</sup>, Shu-Shen Li<sup>a</sup> and Jingbo Li<sup>a,\*</sup>

Received (in XXX, XXX) Xth XXXXXXXXXX 20XX, Accepted Xth XXXXXXXXXX 20XX

DOI: 10.1039/b000000x

Layered GaS nanosheets have been attracting increasing research interests due to their highly anisotropic structural, electrical, optical, and mechanical properties, which are more useful for many applications. However, comparable single-layer or few-layer GaS-based photodetectors have been rarely reported. Here few-layer GaS two-terminal photodetector with fast and stable response has been fabricated. It shows different photo-responses in various of gas environment. Higher photo-response (64.43A/W) and external quantum efficiency (EQE)(12621%) is obtained in ammonia (NH<sub>3</sub>) than that in air or oxygen(O<sub>2</sub>). Theoretical investigation exhibits that charge transfer between the adsorbed gas molecules and photodetector leads to the different photo-responses.

## 1 Introduction

Two-dimensional (2D) materials have attracted significant attention from the scientific community, relating to their potential exotic transport physics and prospects for various technological applications.<sup>1</sup> 2D materials based nanodevices in electronic fields are in favor of further miniaturization beyond Moore's Law and they can serve as a high-mobility option applied in the large-area and low-cost electronic devices.<sup>2,3</sup> Graphene is the most widely studied 2D material so far because of its unusual electrical, magnetic, optical and mechanical properties.<sup>4-6</sup> However, several problems remain with graphene due to absence of a bandgap, which is essential for many applications. For example, graphene can hardly be applied in photodetectors or photoswitching microdevices which need definite on-and-off states.<sup>7</sup> As analogues of graphene, layered transition metal dichalcogenides (TMDs) consisted of one layer transition metal atoms (M) sandwiched between two layers of chalcogen atoms (X) have been regarded as promising materials. Combining chalcogen (X=S, Se, or Te) with transition metal (M=Mo, W, Nb, Re, Ni, Ta, Ti, Zr, Hf or V), TMDs can form in dozens of different categories.<sup>8,9</sup> TMDs with strong X-M-X intralayer covalent bonding within the layers and weak interlayer interaction (van der Waals in nature) have been studied with much attention in view of their great potential in many fields.<sup>9</sup> The preparation, isolation and rapid characterization of layered GaS and other TMDs as well as their optical contrast on various Si/SiO<sub>2</sub> substrates have been reported. It was benefit for the in-depth exploration and potential applications.<sup>10</sup>

Developing novel photodetectors have an important

significance in the progress of optoelectronics field. Among a crowd of various photodetectors, the low dimensional materials based photodetectors are very grateful because of their compact size and easy of manipulation. It is well-known that low dimensional materials with large surface-to-volume ratio can yield higher photosensitivity than their bulk counterparts and the lifetime of photo-generated carriers is considerably prolonged because of charge separation.<sup>11</sup> Some TMDs layered material photodetectors have been developed and much used in recent years, because of their easy to fabricate some complex structures. GaS nanosheet photodetectors made on SiO<sub>2</sub>/Si substrates and flexible polyethylene terephthalate (PET) substrates exhibit a photoresponsivity at 254 nm up to 4.2 A/W and 19.2 A/W, respectively, which is better than some other 2D material based devices.<sup>11,12</sup> O. Lopez-Sanchez demonstrates ultrasensitive monolayer MoS<sub>2</sub> phototransistors which show a maximum external photoresponsivity of 880 A/W at a wavelength of 561 nm and a photo-response in the 400–680 nm range.<sup>8</sup> This is due to their improved mobility, good contact quality and positioning technique. The high surface-to-volume ratio is also useful for new sensor materials which must exhibit selectivity to the analytes, rapid response and recovery, and sensitive transduction of the measured parameters without interference.<sup>3</sup> Field-effect transistor (FET) sensors based on multilayer MoS<sub>2</sub> films exhibit a high sensitivity to NO with detection limit of 0.8 ppm due to their large specific surface areas.<sup>13</sup> The MoS<sub>2</sub> transistors with different thicknesses are assessed for gas-sensing performances with exposure to NO<sub>2</sub>, NH<sub>3</sub>, and humidity in different conditions such as gate bias and light irradiation.<sup>14</sup>

Recent years, considerable progress has been made for the fabrication of different layer-structured III-VI semiconductors in various forms via several techniques in controlled manner, such as micromechanical cleavage, epitaxial growth, chemical vapor deposition, and liquid exfoliation.<sup>15-19</sup> Various high-quality GaS nanostructures as well as other kinds of GaS products have been controlled synthesis via a simple vapor-solid method.<sup>16</sup> Among the III-VI group of semiconductor materials, GaS is one of the most important materials. It has two different stoichiometries, i.e., GaS and Ga<sub>2</sub>S<sub>3</sub>. It is well known that hexagonal GaS has layered structures with each layer consisting of S-Ga-Ga-S repeating unit built by six membered Ga<sub>3</sub>S<sub>3</sub> rings.<sup>20</sup> Layered GaS, with indirect band gap of 2.5 eV, is more useful for applications in photoelectric devices, electrical sensors, and nonlinear optical applications, owing to its highly anisotropic structural, electrical,

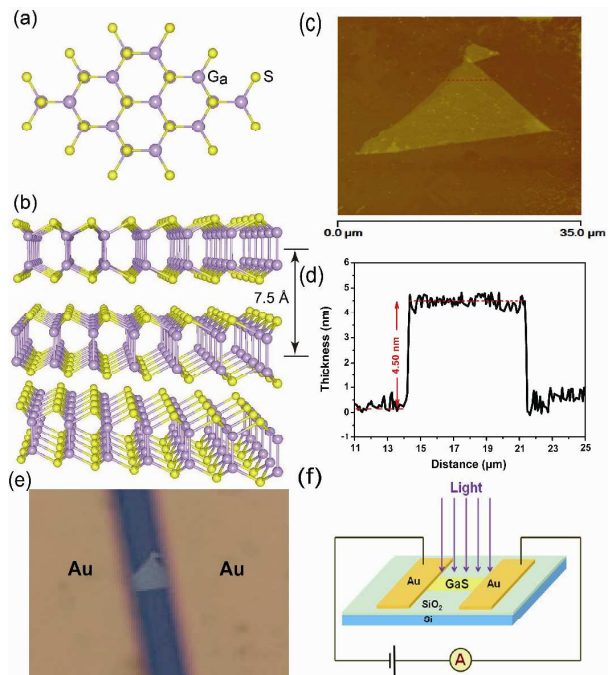


**Figure 1.** (a) The top view and (b) side view of GaS nanosheet, (c) AFM image and (d) a height profile of the few-layer GaS nanosheet, (e) optical image of the device and (f) schematic of the device operation.

optical, and mechanical properties.<sup>16</sup> Doped GaS can be used for the fabrication of near-blue-light emitting devices. The photoluminescence yield for thin films of GaS deposited on GaAs substrate are higher than that of GaAs.<sup>21</sup> Single-sheet of GaS exhibits field-effect respective differential mobilities of  $\sim 0.1$   $\text{cm}^2\text{V}^{-1}\text{s}^{-1}$  along with good On/Off current ratios in the range of  $\sim 10^4$ - $10^5$ .<sup>1</sup> However, comparable single-layer or few-layer GaS-based photodetectors have been rarely reported.

In this communication, we report the design of few-layer GaS photodetectors. The ultrathin GaS nanosheets mechanically exfoliated on a  $\text{SiO}_2/\text{Si}$  substrate are characterized by atomic force microscopy (AFM) and Raman spectroscopy. After deposition of Au electrodes, the two-terminal photodetectors are fabricated. The fabricated GaS photodetector shows different photo-responses in various of gas environment. It has higher current On/Off ratio, photo-response and EQE in  $\text{NH}_3$  environment than that in air or in  $\text{O}_2$ . The photo-response time is around 10 ms, and it still shows good stability after dozens of switching cycles. The unique characteristics of prompt photoswitching, fast response time and good photoresponsivity from the GaS photodetector pave the way for the fabrication of multifunctional and high performance flexible photodetectors and gas sensors based on the layered semiconducting materials in the future.

## 2 Results and discussion

Crystals of GaS are composed of vertically stacked, weakly interacting layers held together by van der Waals interactions (Figure 1a) and the thickness of a single layer is  $\sim 7.5$  Å (Figure 1b).<sup>11</sup> It has a stable, hexagonal, double-layered structure with bond distances of 2.48 Å and 2.37 Å for the Ga–Ga and Ga–S bond lengths, respectively.<sup>16</sup> The micromechanical cleavage technique has been used to fabricate different-layer GaS sheets by

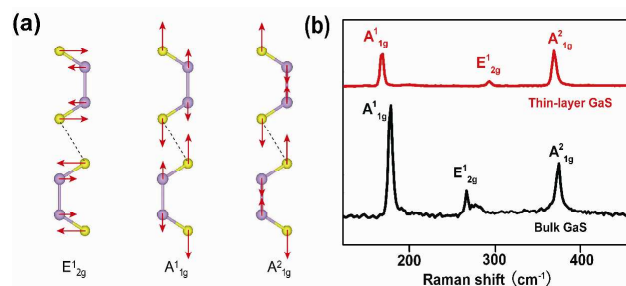


**Figure 2.** (a) Schematic illustration of phonon modes in first-order Raman spectroscopy, and (b) Raman spectroscopy of bulk and few-layer of GaS.

repeatedly peeling the bulk material and transferring this peeled material on top of a  $\text{SiO}_2/\text{Si}$  substrate using adhesive tape. This technique has been proven to be an easy and very fast way of producing highly crystalline and large size sheets of single and few layers.<sup>1</sup> A few-layer nanosheet of GaS derived from micromechanical cleavage from bulk crystal of GaS is shown in Figure 1c, corresponding to AFM image of GaS few layers peeled on 300 nm  $\text{SiO}_2/\text{Si}$  substrates. A height profile along the dashed line in Figure 1c is depicted in Figure 1d. It is noted that the ultrathin GaS nanosheet has a thickness of 4.5 nm, indicating  $\sim 6$  layers of GaS. As shown in Figure 1e, a pair of Au electrodes ( $\sim 50$  nm thick) with 28  $\mu\text{m}$  apart is evaporated by laying a micrometer-sized diametral Au wire as the mask on top of the few-layer GaS peeled on a Si substrate with 300 nm  $\text{SiO}_2$  insulating top layer to obtain a gap between two electrodes. After the evaporation of electrodes, the Au wire mask is removed so that the sample in gap area can be exposed.

Raman spectroscopy is a convenient tool for nondestructive characterization and identification of few-layer materials. Three phonon modes exist in the first-order Raman spectroscopy of GaS nanosheet, *i.e.*  $A_{1g}^1$ ,  $E_{2g}^1$ , and  $A_{2g}^1$  as shown in Figure 2a. Figure 2b shows the comparative Raman spectra of bulk and few-layer of GaS. Typically bulk GaS shows Raman modes  $A_{1g}^1$  (186.89  $\text{cm}^{-1}$ ),  $E_{2g}^1$  (288.91  $\text{cm}^{-1}$ ), and  $A_{2g}^1$  (368.37  $\text{cm}^{-1}$ ). The frequencies shifts of the few-layer GaS Raman modes at room temperature are found to be  $A_{1g}^1$  (183.41  $\text{cm}^{-1}$ ),  $E_{2g}^1$  (297.35  $\text{cm}^{-1}$ ), and  $A_{2g}^1$  (365.28  $\text{cm}^{-1}$ ). As shown in Figure 2a, the frequency of the  $E_{2g}^1$  mode of few-layer GaS increases and that

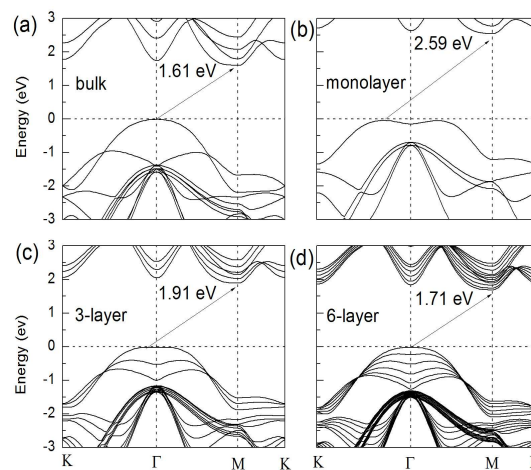


**Figure 3.** The calculated band structures of GaS (a) bulk and nanosheets of (b) monolayer, (c) 3-layer and (d) 6-layer.

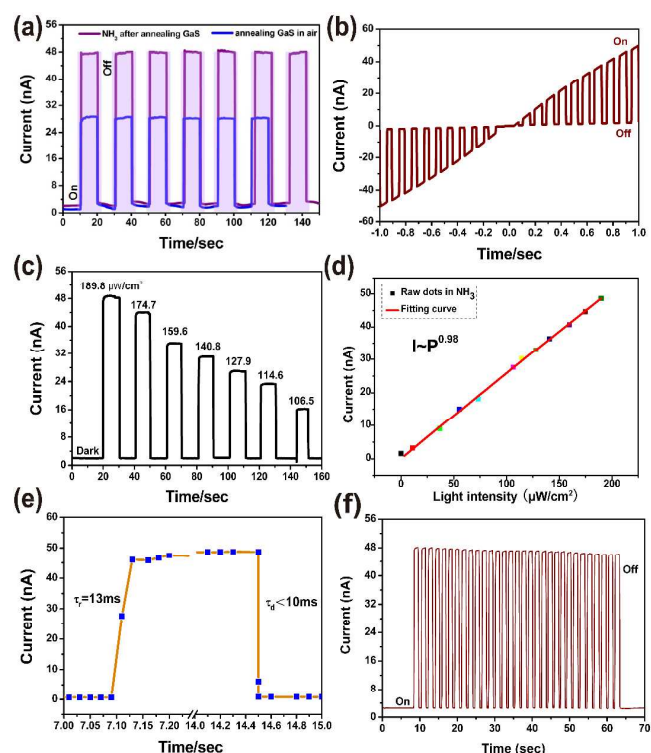


**Figure 4.** (a) Time-resolved photocurrent of the photodetector in response to light on/off in different gas environment (the bias voltage between two electrodes is kept constant at 1 V), (b) I-V curve when the photodetector is alternating illuminated with 633 nm light on/off at an irradiance of 189.8 μW/cm<sup>2</sup> in NH<sub>3</sub> gas, (c) the photocurrent-time curve with the change of light intensity, (d) experimental data fitting of photocurrent-time curve with the change of light intensity, (e) the photocurrent responses with time under illumination of 633 nm in NH<sub>3</sub> environment, (f) representative switching cycles in NH<sub>3</sub> with 1 V bias when 633 nm laser was switched on and off repeatedly.

of A<sub>1g</sub> and A<sub>2g</sub> mode decreases, which corresponds well with the reported Raman spectrum in the ultrathin GaS nanosheet.<sup>11</sup> The energy-dispersive x-ray (EDX) is used to analyze the composition of the few-layer GaS nanosheet, as shown in Figure S1 (Supporting information).

β-phase GaS with experimental lattice constant  $a = 3.585 \text{ \AA}$  is used for band structure calculations,<sup>22</sup> as illustrated in Figure 1. The calculated band structures of GaS bulk and nanosheets of monolayer, 3-layer and 6-layer are shown in Figure 3. The valence band maximum (VBM) and conduction band minimum (CBM) of GaS bulk are located at  $\Gamma$  and M point, respectively, resulting an indirect band gap of 1.61 eV, agreeing with previous theoretical result.<sup>11</sup> Interesting change occurs to VBM when GaS undergoes dimensionality change. The VBM slightly moves along  $\Gamma - K$  direction for nanosheets from monolayer to 5-layer with the energy difference between the VBM and  $\Gamma$  point within 0.11 eV. The CBMs of nanosheets are located at M point without change. For GaS monolayer, the band gap is 2.59 eV, consistent with previous work.<sup>11</sup> The second CBMs of GaS are located at  $\Gamma$  with small energy difference between the second VBM and VBM less than 0.16 eV, therefore, great direct  $\Gamma - \Gamma$  transition probability can be expected.

We probed the devices (Figure 1f) and their time-dependent photo-response to laser excitation using a focused laser beam ( $\lambda = 633 \text{ nm}$ ) as an irradiation source under different gas

environments (NH<sub>3</sub>, air and O<sub>2</sub>). Before we filled with NH<sub>3</sub> or O<sub>2</sub> in the measurement system, the test system was firstly evacuated to exclude interference from other gases in air. The power of the light could be controlled from  $\sim 106.5$  to  $189.8 \text{ μW/cm}^2$ . The bias voltage between two electrodes was kept constant at 1 V. Figure 4a displayed the photocurrent versus time plots of the device irradiated by 633 nm light with light intensity of  $189.8 \text{ μW/cm}^2$  in air and NH<sub>3</sub> gas environment, respectively. The irradiation source was switched on and off periodically at 10 s intervals. From the curve, it could be seen that the device exhibited excellent photo-response properties. Under air environment, the dark current was around 1.5 nA. However, under red light irradiation, the photocurrent could approach 28 nA with a current On/Off ratio of around 18.6. In NH<sub>3</sub> environment, the dark current was  $\sim 2 \text{ nA}$ , the photocurrent was 48 nA and the On/Off ratio was around 24. We have also measured the photo-response in O<sub>2</sub> gas environment, the dark current was  $< 1 \text{ nA}$ , then after irradiated by light, photocurrent jump of  $\sim 7 \text{ nA}$  was obtained. However, in vacuum, the photo-response was higher than that in air (as shown in Supporting information, Figure S2). The photocurrent intensity and current On/Off ratio in NH<sub>3</sub> was much higher than that in air or in O<sub>2</sub>. And for NH<sub>3</sub> gas environment, with the light irradiation on and off, the photo-response emerged three transient regimes: a sharp rise, steady state, and sharp decay. The current increased very sharply from one state to another state, indicating a very fast response speed of the device. When irradiated by red light in NH<sub>3</sub>, the photocurrent quickly increased to a saturated value of 50 nA, and then dramatically decreased to its initial value during the light was turned off (Supporting information Figure S3). Current-voltage (I-V) characteristic measured by switching on/off the red light ( $189.8 \text{ μW/cm}^2$ ) in NH<sub>3</sub> was shown in Figure 4b. Connecting the curves in dark and/or under light illumination, respectively, we noted that both I-V curves in dark and under light illumination were nearly linear, which indicated a good Ohmic contact. The relationship between the photocurrent ( $I_{\text{photo}} = I_{\text{light}} - I_{\text{dark}}$ ) and the light intensity was also investigated. Figure 4c showed that the photocurrent step-like increased as the light intensity was enhanced. The photocurrent was linearly proportional to the incident irradiation intensity within the range of  $\sim 106.5$  to  $189.8 \text{ μW/cm}^2$ . Within the linear range, the few-layer GaS nanosheet should be a typical photon-dependent resistor that the more photons would generate more photocarriers.<sup>23,24</sup> The experimental data of photocurrent-time curve could be best fitting by using the power law  $I_{\text{photo}} = AP_{\lambda}^{\beta}$ , where A was the proportionality constant;  $\beta$  was an exponent that determined the response of  $I_{\text{photo}}$  on the incident light intensity ( $P_{\lambda}$ ). Under NH<sub>3</sub> environment,  $I_{\text{photo}}$  exhibited a intensity dependence of  $\sim 0.98$  as shown in Figure 4d, indicating a high efficient generation of carriers transferred from photons. Response time and repeatability also were key parameters to determine the capability of a photodetector. It was still a challenge to achieve photodetectors with both high photosensitivity and fast lasting response up to date. Figure 4e showed the photo-response of the device under the illumination (633 nm and  $189.8 \text{ μW/cm}^2$ ) in NH<sub>3</sub> environment. The dynamic response to the light illumination for rise and decay could be expressed by  $I(t) = I_0 [1 - \exp(-t/\tau_r)]$  and  $I(t) = I_0 \exp(-t/\tau_d)$ , where  $\tau_r$  and  $\tau_d$  were the time constants for the rise and decay

edges, respectively.<sup>25,26</sup> We noted that the photocurrent rise

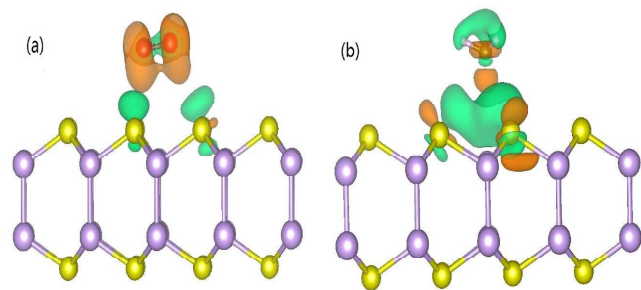


**Figure 5.** A gas molecule adsorbed on the GaS monolayer. Charge density difference between pristine GaS and (a) O<sub>2</sub>-adsorbed and (b) NH<sub>3</sub>-adsorbed GaS monolayer. The iso-surface is for electron density of  $6 \times 10^{-4} \text{ e}/\text{\AA}^3$ . Brown denotes charge accumulation and green denotes charge depletion.

and decay for our device was very steep;  $\tau_r$  and  $\tau_d$  could be estimated to be 13 and  $\sim 10$  ms, respectively. Representative switching cycles in NH<sub>3</sub> with 1 V bias when 633 nm laser was switched on and off repeatedly was shown in Figure 4f. After multiple illumination cycles, the photocurrent still responded in a similar fashion to the light, which demonstrated the high robustness and good reproducibility of the photodetectors.

The photoresponsivity ( $R_\lambda$ ) and the EQE were both critical parameters for photodetectors, which determined sensitivity for an optoelectronic device.  $R_\lambda$  was defined as the photocurrent generated per unit power of incident light on the effective area of a photodetector. EQE was defined as the number of carriers circulating through a photodetector per adsorbed photon and per unit time,  $R_\lambda$  and EQE could be calculated in the following equations:  $R_\lambda = \Delta I_\lambda / (P_\lambda S)$  and  $\text{EQE} = hcR_\lambda / (e\lambda)$ , where  $\Delta I_\lambda = I_{\text{light}} - I_{\text{dark}}$  was the photocurrent,  $S$  was the effective illuminated area,  $h$  was Planck's constant,  $c$  was the light velocity,  $e$  was the electronic charge, and  $\lambda$  was the incident light wavelength.<sup>23,26,27</sup> For our device,  $\Delta I_\lambda = 4.6 \times 10^{-8} \text{ A}$ ,  $P_\lambda = 189.8 \text{ }\mu\text{W}/\text{cm}^2$ ,  $S = \sim 376.32 \text{ }\mu\text{m}^2$ ,  $\lambda = 633 \text{ nm}$ , then  $R_\lambda$  and EQE could be estimated to be about 64.43 A/W and 12621%, respectively. The parameters of the GaS photodetector compared to other optoelectronic devices were shown in Table 1. The photo-response of our device was higher than the pure monolayer graphene photodetector (8.61 A/W)<sup>32</sup> and graphene nanoribbons (1 A/W).<sup>33</sup> But the response time was still slower than the graphene photodetectors.<sup>34</sup> And graphene based device had a broad operation spectrum (from 1.35 to 1.6  $\mu\text{m}$ ) under ambient conditions.<sup>35</sup>

To investigate the influence of gas adsorption on photosensitivity, the interactions between GaS monolayer and NH<sub>3</sub> or O<sub>2</sub> were simulated using First-principles calculations. Extensive tests about the adsorbing positions and the gap molecular configurations revealed that NH<sub>3</sub> (O<sub>2</sub>) was physisorbed above Ga atom on the monolayer with a 156.1 meV (102.55 meV) binding energy. Approximately, 0.02 electrons per NH<sub>3</sub> were transferred from NH<sub>3</sub> to GaS monolayer, while 0.07 electrons per O<sub>2</sub> were transferred from GaS monolayer to O<sub>2</sub>, therefore, NH<sub>3</sub> served as donor but O<sub>2</sub> acted as acceptor. Moreover, the transferred charges were more localized around adsorbed O<sub>2</sub> than adsorbed NH<sub>3</sub>, which was demonstrated in Figure 5. Brown denoted charge accumulation in O<sub>2</sub> and green denoted charge depletion in NH<sub>3</sub> (Figure 5). It proved that NH<sub>3</sub>

lost electrons to GaS and O<sub>2</sub> captured electrons from GaS. To enhance the sensitivity to gas environment, an annealing process was needed for the few-layer GaS nanosheet. Here, the annealing could be applied to thermally drive away contaminants/organic residue, simultaneously, it might be creating a small density of chalcogen vacancies.<sup>28</sup> After the annealing process, the photocurrent intensity of the nanosheet became extremely sensitive to gas environment as shown in Figure 4. We also calculated the charge transfer under NH<sub>3</sub> environment after the generation of chalcogen vacancies. The result showed that 0.12 electrons per NH<sub>3</sub> were transferred from NH<sub>3</sub> to GaS monolayer. And after the generation of chalcogen vacancies, the structure of GaS changed, resulting in the increase of the adsorption energy, the decrease of the distance between NH<sub>3</sub> molecule and GaS monolayer, and the enhancement of charge transfer from NH<sub>3</sub> to GaS (shown in Supporting information Figure S4). Since the mechanically exfoliated GaS nanosheet was a n-type semiconductor with background free electrons coming probably from defects, the adsorption of NH<sub>3</sub> further transferred electrons to the nanosheet and increased its carrier density.<sup>28,29</sup> When irradiated by light, the GaS nanosheet strongly absorbed the photons, and electron-hole pairs generated in the nanosheet. Under the external electric field, the photogenerated carriers moved in direction and were separated, resulting in the generation of photocurrent. When the device performed in NH<sub>3</sub> environment, the adsorption of NH<sub>3</sub> could increase the carrier density of the GaS nanosheet due to electron transfer, so we noted that the photo-response in NH<sub>3</sub> gas was better than that in air (Figure 4b). But when measured in O<sub>2</sub>, because of the reversed electron transfer from GaS to O<sub>2</sub> and the decrease of carrier density, the photo-response of the device was greatly weakened. Therefore, the device exhibited much better photosensitive property in NH<sub>3</sub> environment than that in air or O<sub>2</sub>. And for vacuum, there was no adsorbed gases (like O<sub>2</sub>) interference and electron transfer between the surrounding environment and GaS nanosheet, so the photocurrent was higher than that in air.

Photodetectors	$R_\lambda$ (A W <sup>-1</sup> )	EQE (%)	Response time
Few-layer MoS <sub>2</sub> <sup>30</sup>	0.57		$\sim \mu\text{s}$
Graphene <sup>31</sup>	$1.0 \times 10^{-3}$	6-16	
Monolayer graphene <sup>32</sup>	8.61		$\sim 200 \text{ s}$
Few-layer GaSe sheets <sup>36</sup>	2.8	1367	$\sim 0.02 \text{ s}$
Our photodetector	64.43	12621	$\sim 10 \text{ ms}$

**Table 1.** Comparison of the parameters of few-layer GaS device to the reported 2D material based photodetectors.

## 4 Conclusions

In summary, high performance of few-layer GaS nanosheet photodetectors have been fabricated. The  $R_\lambda$  and EQE of the device were obtained at different gas environments and exhibited  $\sim 64.43 \text{ A W}^{-1}$  and 12621%, respectively, under 633 nm light

irradiation in NH<sub>3</sub> gas. The switching cycles of photocurrent were fast and stable. A theoretical investigation of the effect of NH<sub>3</sub> and/or O<sub>2</sub> adsorption on the photo-response was also performed. These experimental and theoretical findings indicated that the few-layer GaS nanosheet could be used in high-performance nanosensors, photodetectors, photoswitches and optoelectronic circuits.

## Acknowledgment

We thank Prof. Junqiao Wu and Dr. Sefaattin Tongay for the discussion. Prof. Jingbo Li gratefully acknowledges financial support from National Science Found for Distinguished Young Scholar (Grant No. 60925016 and 91233120) and the National Basic Research Program of China (Grant No. 2011CB921901). Dr. Shengxue Yang acknowledges financial support from China Postdoctoral Science Foundation( No. 2013M540127).

## Notes and references

<sup>a</sup> State Key Laboratory of Superlattices and Microstructures, Institute of Semiconductors, Chinese Academy of Sciences, P.O. Box 912, Beijing 100083, China. E-mail: jbli@semi.ac.cn

<sup>b</sup> Zhejiang Provincial Key Laboratory of Solid State Optoelectronic Devices, Zhejiang Normal University, Zhejiang 321004, China.

† Electronic Supplementary Information (ESI) available: [Experimental section, Density Functional Theory Calculations, EDX of GaS nanosheet, I-t curve in O<sub>2</sub> gas environment and in vacuum, Saturated I-t curve in NH<sub>3</sub> gas environment.]. See DOI: 10.1039/b000000x/

- 1 D. J. Late, B. Liu, J. Luo, A. Yan, H. S. S. R. Matte, M. Grayson, C. N. R. Rao and V. P. Dravid, *Adv. Mater.* 2012, **24**, 3549.
- 2 H. Wang, L. Yu, Y. Lee, Y. Shi, A. Hsu, M. L. Chin, L. Li, M. Dubey, J. Kong and T. Palacios, *Nano Lett.* 2012, **12**, 4674.
- 3 F. K. Perkins, A. L. Friedman, E. Cobas, P. M. Campbell, G. G. Jernigan and B. T. Jonker, *Nano Lett.* 2013, **13**, 668.
- 4 A. K. Geim and K. S. Novoselov, *Nat. Mater.* 2007, **6**, 183 .
- 5 A. K. Geim, *Science* 2009, **324**, 1530 .
- 6 C. N. R. Rao, A. K. Sood, K. S. Subrahmanyam and A. Govindaraj, *Angew. Chem. Int. Ed.* 2009, **48**, 7752 .
- 7 H. S. Lee, S. Min, Y. Chang, M. K. Park, T. Nam, H. Kim, J. H. Kim, S. Ryu and S. Im, *Nano Lett.* 2012, **12**, 3695.
- 8 O. Lopez-Sanchez, D. Lembke, M. Kayci, A. Radenovic and A. Kis, *Nature Nanotech.* 2013, **8**, 497.
- 9 M. Xu, T. Liang, M. Shi and H. Chen, *Chem. Rev.* 2013, **113**, 3766.
- 10 D. J. Late, B. Liu, H. S. S. Ramakrishna Matte, C. N. R. Rao and V. P. Dravid, *Adv. Funct. Mater.* 2012, **22**, 1894; V. Stengl and J. Henych, *Nanoscale* 2013, **5**, 3387; W. Ge, K. Kawahara, M. Tsuji and H. Ago, *Nanoscale*, 2013, **5**, 5773.
- 11 P. Hu, L. Wang, M. Yoon, J. Zhang, W. Feng, X. Wang, Z. Wen, J. C. Idrobo, Y. Miyamoto, D. B. Geohegan and K. Xiao, *Nano Lett.* 2013, **13**, 1649.
- 12 Z. Yin, H. Li, L. Jiang, Y. Shi, Y. Sun, G. Lu, Q. Zhang, X. Chen and H. Zhang, *ACS Nano* 2012, **6**, 74.
- 13 H. Li, Z. Yin, Q. He, H. Li, X. Huang, G. Lu, D. W. H. Fam, A. I. Y. Tok, Q. Zhang and H. Zhang, *Small* 2012, **8**, 63.
- 14 D. J. Late, Y. Huang, B. Liu, J. Acharya, S. N. Shirodkar, J. Luo, A. Yan, D. Charles, U. V. Waghmare, V. P. Dravid and C. N. R. Rao, *ACS Nano* 2013, **7**, 4879.
- 15 K. S. Novoselov, A. K. Geim, S. V. Morozov, D. Jiang, Y. Zhang, S. V. Dubonos, I. V. Grigorieva and A. A. Firsov, *Science* 2004, **306**, 666.
- 16 G. Shen, D. Chen, P. Chen and C. Zhou, *ACS Nano* 2009, **3**, 1115.
- 17 C. Berger, Z. Song, T. Li, X. Li, A. Y. Ogbazghi, R. Feng, Z. Dai, A. N. Marchenkov, E. H. Conrad, P. N. First and W. A. de Heer, *J. Phys. Chem. B* 2004, **108**, 19912 .

- 18 R. Rosei, S. Modesti, F. Sette, C. Quaresima, A. Savoia and P. Perfetti, *Phys. Rev. B* 1984, **29**, 3416; Y. C. Lin, W. Zhang, J. K. Huang, K. K. Liu, Y. H. Lee, C. T. Liang, C. W. Chud and L. J. Li, *Nanoscale* 2012, **4**, 6637.
- 19 J. N. Coleman, M. Lotya, A. O'Neill, S. D. Bergin, P. J. King, U. Khan, K. Young, A. Gaucher, S. De, R. J. Smith, I. V. Shvets, S. K. Arora, G. Stanton, H. Kim, K. Lee, G. T. Kim, G. S. Duesberg, T. Hallam, J. J. Boland, J. J. Wang, J. F. Donegan, J. C. Grunlan, G. Moriarty, A. Shmeliov, R. J. Nicholls, J. M. Perkins, E. M. Grieveson, K. Theuwissen, D. W. McComb, P. D. Nellist and V. Nicolosi, *Science* 2011, **331**, 568.
- 20 G. Sinha, S. K. Panda, A. Datta, P. G. Chavan, D. R. Shinde, M. A. More, D. S. Joag and A. Patra, *ACS Appl. Mater. Interfaces* 2011, **3**, 2130.
- 21 T. Aono, K. Kase, A. Kinoshita, *J. Appl. Phys.* 1993, **74**, 2818; Q. S. Xin, S. Conrad, X. Y. Zhu, *Appl. Phys. Lett.* 1996, **69**, 1244.
- 22 H. Damour, W. B. Holzapfel, A. Polian and A. Chevy, *Solid State Commun* 1982, **44**, 853.
- 23 Z. Wang, M. Safdar, C. Jiang and J. He, *Nano Lett.* 2012, **12**, 4715.
- 24 Q. L. Li, Y. Li, J. Gao, S. D. Wang and X. H. Sun, *Appl. Phys. Lett.* 2011, **99**, 243105.
- 25 Y. Liang, H. Liang, X. Xiao and S. Hark, *J. Mater. Chem.* 2012, **22**, 1199.
- 26 Y. Zhang, W. Deng, X. Zhang, X. Zhang, X. Zhang, Y. Xing and J. Jie, *ACS Appl. Mater. Interfaces* 2013, DOI: 10.1021/am402087v.
- 27 L. Hu, J. Yan, M. Liao, H. Xiang, X. Gong, L. Zhang and X. Fang, *Adv. Mater.* 2012, **24**, 2305.
- 28 S. Tongay, J. Zhou, C. Ataca, J. Liu, J. S. Kang, T. S. Matthews, L. You, J. Li, J. C. Grossman and J. Wu, *Nano Lett.* 2013, **13**, 2831.
- 29 S. Y. Hu, Y. Z. Chen, K. K. Tiong and Y. S. Huang, *Materials Chemistry and Physics* 2007, **104**, 105; Q. Yue, Z. Shao, S. L. Chang and J. Li, *Nanoscale Res. Lett.* 2013, **8**, 425.
- 30 D. Tsai, K. Liu, D. Lien, M. Tsai, C. Kang, C. Lin, L. Li and J. He, *ACS Nano* 2013, **7**, 3905.
- 31 F. Xia, T. Mueller, Y. Lin, A. Valdes-Garcia and P. Avouris, *Nat. Nanotechnol.* 2009, **4**, 839.
- 32 Y. Zhang, T. Liu, B. Meng, X. Li, G. Liang, X. Hu and Q. Wang, *Nat. Commun.* 2013, **4**, 1811.
- 33 B. Chitara, L. S. Panchakarla, S. B. Krupanidhi, and C. N. R. Rao, *Adv. Mater.* 2011, **23**, 5419.
- 34 A. Urich, K. Unterrainer and T. Mueller, *Nano Lett.* 2011, **11**, 2804.
- 35 M. Liu, X. Yin, E. Ulin-Avila, B. Geng, T. Zentgraf, L. Ju, F. Wang and Xiang Zhang, *Nature* 2011, **474**, 64.
- 36 P. Hu, Z. Wen, L. Wang, P. Tan and K. Xiao, *ACS Nano* 2012, **6**, 5988.